Soft Matter

RSC Publishing

PAPER

View Article Online
View Journal | View Issue

Cite this: *Soft Matter*, 2013, **9**, 5196

Supramolecular structures of uracil-functionalized PEG with multi-diamidopyridine POSS through complementary hydrogen bonding interactions†

Jui-Hsu Wang,[a] Oleksii Altukhov,[b] Chih-Chia Cheng,[a] Feng-Chih Chang*[ab] and Shiao-Wei Kuo*[b]

Received 29th December 2012
Accepted 28th March 2013

DOI: 10.1039/c3sm27968e

www.rsc.org/softmatter

In this study, we synthesized (i) a multi-diamidopyridine-functionalized polyhedral oligomeric silsesquioxane (MD-POSS) through nucleophilic substitution and click 1,3-cycloaddition reactions and (ii) both mono- and bis-uracil (U)-functionalized poly(ethylene glycol) derivatives (U–PEG and U–PEG–U, respectively) through Michael additions of U to acryloyl-functionalized PEG oligomers. Transmission electron microscopy (TEM) and dynamic light scattering (DLS) revealed that supramolecular structures self-assembled from mixtures of MD-POSS and U–PEG and from MD-POSS and U–PEG–U. Fourier transform infrared (FTIR) and nuclear magnetic resonance (NMR) spectroscopy confirmed the presence of multiple hydrogen bonding interactions between the diaminopyridine groups of MD-POSS and the U groups of U–PEG and U–PEG–U. Because of these strong reversible intermolecular multiple hydrogen bonds, the POSS-based polymer-like supramolecular materials exhibited improved thermal properties upon increasing the MD-POSS content.

Introduction

Supramolecular polymers are polymeric materials formed through self-assembly with stabilizing non-covalent interactions.[1] In biology, complexity and molecular function arise through Nature's efficient use of non-covalent bonds to form advanced polymeric architectures from such species as DNA and proteins. In polymer science, however, functional materials are mainly prepared through covalent bonding, with limited use of self-assembly as a chief design motif. Whereas almost all non-covalently stabilized materials in Nature feature multiple self-assembly motifs, the majority of synthetic systems employ only a single self-assembly motif. Many recognition motifs and non-covalent forces have, however, been reported for supramolecular polymers, ranging from π–π interactions and hydrogen bonding to metal coordination and electrostatic interactions.[2–4]

The multiple hydrogen bonding interactions found in DNA and RNA are useful for organizing novel structures through selective complementary nucleobase recognition [*e.g.*, thymine–adenine (T–A), cytosine–guanine (C–G), and uracil–adenine (U–A) complexes].[5–7] Similar to the specific self-recognition properties of DNA and RNA strands and their widespread applications in various aspects of biotechnology and nanotechnology,[8,9] nucleobase-functionalized synthetic polymers can also form interesting structures for advanced applications.[10–13] Indeed, several reports have appeared on nucleobase functionalities introduced into main- and side-chain polymers to form assemblies that take advantage of biocomplementary hydrogen bonding.[14–16] In addition, some studies have investigated the biocomplementary interactions between nucleobase-like side-chain homopolymers and alkylated nucleobases, stabilized by T–A and U–A base pairs.[17,18] Such approaches can be used to prepare well-defined polymers having a broad range of applications.[19,20] The synthesis and utility of synthetic polymers bearing complementary nucleobases is an interesting subject in polymer science and will likely expand further in the future.

Recent years have witnessed the development of novel classes of organic/inorganic hybrid materials based on polyhedral oligomeric silsesquioxane (POSS) nanoparticles.[21–28] Relative to other nanofillers, POSS derivatives have the advantages of monodisperse molecular weight, well-defined structure, low density, high temperature stability, the absence of trace metals, and sizable interfacial interactions in composite particles and with polymer segments.[21] Through appropriate design of the structure, these POSS derivatives can be tailored for specific applications. Jeounge *et al.* and Carroll *et al.* used a POSS derivative with one diaminopyridine arm to self-assemble,

[a]*Institute of Applied Chemistry, National Chiao Tung University, 30010 Hsinchu, Taiwan. E-mail: changfc1973@gmail.com*

[b]*Department of Materials and Optoelectronic Science, National Sun Yat-Sen University, 804 Kaohsiung, Taiwan. E-mail: kuosw@faculty.nsysu.edu.tw*

† Electronic supplementary information (ESI) available. See DOI: 10.1039/c3sm27968e

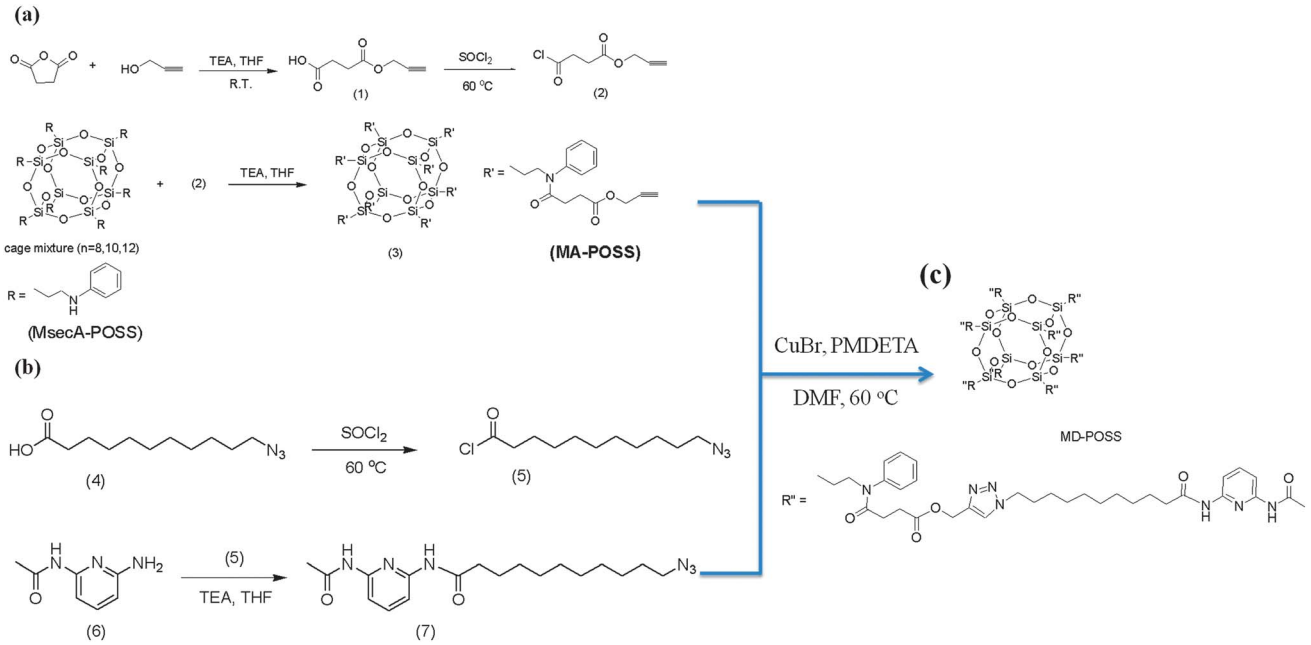

Scheme 1 Synthesis of MD-POSS.

through thymine-functionalized monolayers, onto gold surfaces and polystyrene matrices.[29,30] Cheng *et al.* reported that the eight diaminopyridine arms of a POSS derivative could self-assemble—through self-quadruple hydrogen bonding interactions—to form physically cross-linked polymer-like structures.[31]

In this study, we synthesized a multi-diaminopyridine-functionalized POSS derivative (MD-POSS) through click reactions of a multi-propynyl-functionalized POSS with an azido-functionalized diaminopyridine (Scheme 1). We also prepared mono- and bis-U-functionalized poly(ethylene glycol) (PEG) derivatives through Michael reactions of acryloyl–PEG derivatives with U moieties (Scheme 2). We then used differential scanning calorimetry (DSC), Fourier transform infrared (FTIR) spectroscopy, nuclear magnetic resonance (NMR) spectroscopy, and transmission electron microscopy (TEM) to characterize the supramolecular structures self-assembled from MD-POSS and U–PEG and from MD-POSS and U–PEG–U and stabilized through multiple hydrogen bonding interactions.

Experimental

Materials

Propargyl alcohol, succinic anhydride, hydrazine, acrylate–PEG (M_n = 350 g mol^{-1}) and methacrylate–PEG (M_n = 360 g mol^{-1}) were obtained from Aldrich Chemical. Triethylamine was purchased from TEDIA. Thionyl chloride was obtained from TCI-UK. Sodium azide, diaminopyridine, acetic anhydride, copper bromide, *N*,*N*,*N*′,*N*″,*N*″-pentamethyl diethylenetriamine and potassium *tert*-butoxide were purchased from Acros Organics. Acryloyl chloride and U were obtained from Alfa Aesar. A mixture of *N*-phenylaminopropyl POSS cage derivatives was purchased from Hybrid Plastics. All solvents for high-performance liquid chromatography (HPLC) were obtained from TDCI.

Synthesis of MD-POSS

4-Oxo-4-(prop-2-ynyloxy)butanoic acid (1). Propargyl alcohol (40.0 g, 0.741 mol), DMAP (17.4 g, 0.143 mol), and succinic anhydride (85.7 g, 0.856 mol) were dissolved in DCM (100 mL) and reacted overnight under an Ar atmosphere at 25 °C. Water (75 mL) was added and then the organic phase was washed three times with 10% $NaHSO_4$, dried ($MgSO_4$), filtered, and concentrated to give a transparent colorless powder. Yield: 82% (107.6 g). ^{1}H NMR ($CDCl_3$, 300 MHz) δ 2.48 (t, 1H, C*H*), 2.62–2.70 (m, 4H, CH_2C=O), 4.67 (d, 2H, OCH_2CCH); ^{13}C NMR ($CDCl_3$, 300 MHz) δ 28.46, 28.67, 52.23, 75.05, 77.27, 171.32, 178.19. EI$^+$-MS: *m*/*z* 157 (calcd: 156.14). M.p.: 62.5 °C.

(Prop-2-ynyl 4-oxo-4-(phenyl(propyl)amino)butanoate) POSS cage mixture (3). Compound **1** (30.0 g, 0.192 mol) was added to a reaction flask equipped with a reflux condenser and purged with three vacuum/Ar cycles. After heating at 60 °C to melt compound **1**, thionyl chloride (45.7 g, 0.384 mol) was added slowly and then the mixture was stirred for 2 h at 60 °C. After 2 h, the excess thionyl chloride was removed through rotary evaporation; the product (**2**), a light-yellow liquid, was stored under Ar. Yield: 95%.

A mixture of *N*-phenylaminopropyl POSS cage derivatives (2.83 g, 1.90 mmol) was added to a three-neck flask, which was purged with three vacuum/Ar cycles, and then it was dissolved in dry THF (200 mL) and TEA (0.280 g, 2.85 mmol) and cooled in an ice bath. A solution of compound **2** in dry THF (50 mL) was placed in the feed-pipe and then slowly added dropwise into the three-neck flask. The mixture was left at room temperature overnight and then the solvent was removed using a rotary evaporator. The residue was dissolved in EtOAc and washed three times with saturated $NaHCO_3$; the organic phase was dried ($MgSO_4$) and concentrated using a rotary evaporator. The residue was purified chromatographically (EtOAc–CH_2Cl_2, 1 : 3;

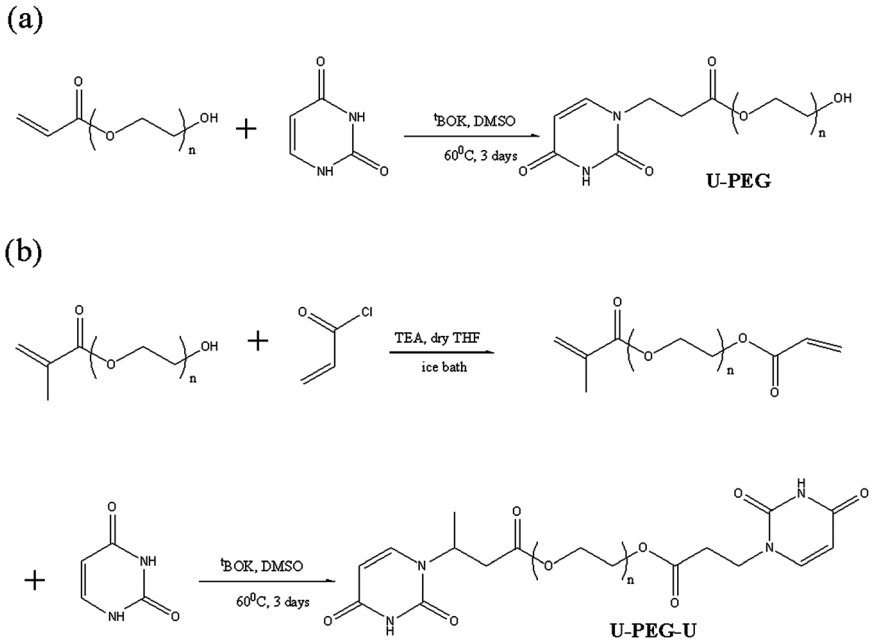

Scheme 2 Synthesis of (a) U–PEG and (b) U–PEG–U.

$R_f = 0.64$) to give a red viscous liquid (**3**); yield: 89%. ^{1}H NMR ($CDCl_3$, 300 MHz) δ 7.33 (m, 4H, C_6H_6), 7.13 (d, 1H, C_6H_6), 4.60 (d, 2H, OCCH_2CCH), 3.51 (t, 2H, CH_2CH_2N), 2.57 (m, 2H, O=CCH_2CH_2), 2.42 (s, 1H, OCCH_2CCH), 2.27 (m, 2H, CH_2CH_2C=O), 1.36 (m, 2H, $CH_2CH_2CH_2$), 0.56–0.09 (m, 2H, SiCH_2CH_2).

11-Azidoundecanoic acid (4). Sodium azide (4.91 g, 75.4 mmol) was added to a solution of 11-bromoundecanoic acid (10.0 g, 37.7 mmol) in DMSO, and then the mixture was stirred overnight under an Ar atmosphere at room temperature. After evaporating the solvent through vacuum distillation, the residue was partitioned between EtOAc and saturated $NaHCO_3$ solution; the organic phase was dried ($MgSO_4$) and concentrated using a rotary evaporator to give a white solid; yield: 99%. M.p.: 34.4 °C. ^{1}H NMR ($CDCl_3$, 300 MHz) δ 11.28 (s, 1H, OH), 3.21 (t, 2H, HOOCCH_2CH_2), 2.31 (t, 2H, $CH_2CH_2CH_2$), 1.67–1.46 (m, 12H, $CH_2C_6H_{12}CH_2$), 1.29 (m, 4H, $C_2H_4N_3$). ^{13}C NMR ($CDCl_3$, 300 MHz) δ 180.69, 51.63, 34.29, 29.69, 29.41, 29.12, 29.01, 26.88, 24.83.

***N*-(6-Aminopyridin-2-yl)acetamide (6).** Compound **4** (7.00 g, 30.8 mmol) was placed in a reaction flask (equipped with a reflux condenser), which was then subjected to purging through three vacuum/Ar cycles. After the mixture had been heated to 60 °C to melt compound **4**, thionyl chloride (7.32 g, 61.6 mmol) was added and the resultant mixture was stirred for 2 h at 60 °C. After 2 h, the excess thionyl chloride was evaporated and the product (**5**), a light-yellow liquid, was stored under Ar; yield: 95%. Diaminopyridine was dissolved in dry THF (400 mL), subjected to purging through three vacuum/Ar cycles, and then added into a two-neck flask charged with dry TEA (0.925 g, 0.265738 mol). A solution of succinic anhydride in dry THF was placed in a feed-pipe and slowly added dropwise into the flask, the contents of which were then stirred overnight at room temperature. After concentrating using a rotary evaporator, the residue was purified through column chromatography (EtOAc) to provide a white solid (**6**); yield: 52%. M.p.: 166.72 °C. ^{1}H NMR ($CDCl_3$, 300 MHz) δ 7.31 (t, 1H, HC=CHCH), 7.18 (d, 1H, HC=CHC), 6.15 (dd, 1H, HC=CHCH=), 3.45 (s, 2H, NH_2), 2.01 (s, 3H, O=CCH_3). ^{13}C NMR ($CDCl_3$, 300 MHz) δ 174.29, 163.81, 155.85, 144.26, 108.71, 106.28, 29.34.

***N*-(6-Acetamidopyridin-2-yl)-11-azidoundecanamide (7).** Compound **6** (4.20 g, 27.8 mmol) was placed in a three-neck flask, subjected to purging through three vacuum/Ar cycles, and then dissolved in dry THF (200 mL) and dry TEA (4.25 g, 42.1 mmol). A solution of compound **5** in dry THF (50 mL) was placed in the feed-pipe and slowly added dropwise into the three-neck flask, which was cooled in an ice bath. The mixture was stirred overnight at room temperature. The solvent was removed using a rotary evaporator and the residue was partitioned between EtOAc and saturated $NaHCO_3$; the organic phase was dried ($MgSO_4$) and concentrated. The residue was purified through column chromatography to give a light-yellow powder (**7**); yield: 76%. M.p.: 92.25 °C. ^{1}H NMR ($CDCl_3$, 300 MHz) δ 9.99 (d, 1H, O=CNH), 7.67 (m, 3H, C_6H_6), 2.47 (s, 3H, O=CCH_3), 2.35 (t, 2H, O=CCH_2CH_2), 2.06 (s, 2H, $CH_2CH_2C_6H_{12}$), 1.49 (dd, 4H, $C_2H_4N_3$), 1.22 (m, 12H, $CH_2C_6H_{12}CH_2$). ^{13}C NMR ($CDCl_3$, 300 MHz) δ 172.21, 150.37, 139.84, 108.95, 108.82, 50.63, 40.34, 40.07, 38.95, 36.12, 28.59, 28.26, 26.17, 25.00, 24.02.

Diaminopyridine-functionalized POSS cage mixture (MD-POSS). PMDETA (0.25 mL) was added to a solution of compound **7** (5.00 g, 13.9 mmol), compound **3** (3.00 g, 1.14 mmol), and CuBr (0.15 g) in DMF (50 mL) and then the mixture was heated at 80 °C for several hours while being monitored through gel permeation chromatography (GPC; until a shift occurred to a lower elution time and the original peaks disappeared). The DMF was distilled off under vacuum and the

residue was washed several times with diethyl ether to give a light-brown powder (MD-POSS), which was dried under vacuum; yield: 83%. ^{1}H NMR ($CDCl_3$, 300 MHz) δ 1.93–1.57 (m, 12H, $CH_2(CH_2)_6CH_2$), 1.47–1.09 (m, 2H, $CH_2CH_2CH_2C{=}O$), 2.45–2.20 (m, 2H, triazole–$CH_2CH_2(CH_2)_6$), 2.18–2.06 [m, 2H, $CH_2CH_2(C{=}O)NH$], 2.61–2.48 (m, 4H, $O{=}CC_2H_4C{=}O$), 3.58–3.30 [m, 2H, $(O{=}C)PhNCH_2$], 5.24–5.02 [m, 2H, $(O{=})OCCH_2$–pyrrole], 7.15 (m, 2H, octa-C_6H_6), 7.40 (m, 1H, *p*-C_6H_4, triazole–H), 7.72 (m, 2H, *m*-C_6H_4), 7.91 (m, 2H, *m*-C_6H_4), 8.31–8.08 (m, 3H, pyrrole–*H*).

Synthesis of U–PEG

3-(2,4-Dioxo-3,4-dihydro-2*H*-pyrimidin-1-yl)propionic acid 2-hydroxyethyl ester. A solution of PEG–acrylate (17.8 mL, 0.053 mol), U (24.0 g, 0.214 mol), and potassium *tert*-butoxide (1.00 g, 9 mmol) in DMSO (200 mL) in a flask equipped with a Graham condenser was heated on a hot plate (60 °C) for 48 h. After distillation of the DMSO, the solid residue was dissolved in CH_2Cl_2 and filtered. The solvent was evaporated from the filtrate in a rotary evaporator and the residue was dried under vacuum for 24 h; yield: 82%. ^{1}H NMR ($CDCl_3$, 300 MHz) δ 11.24 (1H, OCNHCO), 7.41 (1H, OCCHCHN), 5.63 (1H, HCCHN), 4.21 (2H, NCH_2CH_2COO), 3.97 (2H, $OCOCH_2CH_2$), 3.79–3.33 (mH, OCH_2CH_2O), 2.79 (2H, CH_2CH_2COO), 2.60 (OH), M_n = 534 g mol^{-1}, PDI = 1.02 based on GPC analysis.

Synthesis of U–PEG–U

3-(2,4-Dioxo-3,4-dihydro-2*H*-pyrimidin-1-yl)propionic acid 2-[4-(2,4-dioxo-3,4-dihydro-2*H*-pyrimidin-1-yl)-2-oxo-butoxy]ethyl ester. A solution of acryloyl chloride (7.80 g, 79.5 mmol) in THF was added through a dropping funnel into a solution of PEG–acrylate (17.8 mL, 0.053 mol), triethylamine (11.9 mL, 0.0795 mol), and THF (150 mL) in a 500 mL flask, cooled in an ice bath, and then the mixture was stirred for 24 h. The precursor—collected after centrifugation, filtration, and rotary evaporation of the solvent—was added to a flask containing a solution of U (48.0 g, 0.428 mol) and potassium *tert*-butoxide (1.00 g, 9.00 mmol) in DMSO (200 mL) and then the stirred mixture was heated at 60 °C for 48 h. After distillation of the DMSO, the solid residue was dissolved in CH_2Cl_2, filtered, and concentrated to give the final product, which was dried under vacuum for 24 h; yield: 79%. ^{1}H NMR ($CDCl_3$, 300 MHz) δ 10.27 (2H, OCNHCO), 7.31, 7.19 (2H, OCCHCHN), 5.51 (2H, HCCHN), 4.09 (4H, NCH_2CH_2COO), 3.86 (4H, $OCOCH_2CH_2$), 3.59–3.41 (mH, OCH_2CH_2O), 2.91 (2H, CH_2CHCH_3COO), 2.67 (2H, $COCH_2CH_2N$), 1.09 (3H, $CHCH_3$). M_n = 625 g mol^{-1}, PDI = 1.02 based on GPC analysis.

Supramolecular structures MD-POSS/U–PEG and MD-POSS/U–PEG–U

Blends of MD-POSS and U–PEG or U–PEG–U were prepared through solvent-casting. Desired amounts of MD-POSS and U–PEG or U–PEG–U were dissolved in THF and then stirred at 80 °C for 24 h. The solvents were evaporated slowly from the resultant mixtures at 100 °C for 24 h. The supramolecular films were then dried for an additional 72 h under vacuum at 100 °C.

Characterization

Using appropriate deuterated solvents, ^{1}H NMR spectra were recorded using a Varian Unity Inova 300 FT NMR spectrometer operated at 300 MHz; chemical shifts are reported in parts per million (ppm). Molecular weights and molecular weight distributions were determined through GPC using a Waters 510 HPLC instrument equipped with a 410 differential refractometer, a refractive index (RI) detector, and three Ultrastyragel columns (100, 500, and 10^3) connected in series with increasing pore size (eluent: DMF-d_7; flow rate: 0.6 mL min^{-1}). A Biflex III (Bruker Daltonics) time-of-flight mass spectrometer equipped with a 337 nm nitrogen laser was used to record MALDI-TOF mass spectra of the samples. FTIR spectra (KBr disk method) were measured using a Nicolet Avatar 320 FTIR spectrometer; 32 scans were collected at a resolution of 1 cm^{-1}; the sample chamber was purged with N_2 to maintain film dryness. Thermal analysis was performed using a DSC instrument (TA Instruments Q-20). The sample (*ca.* 4–6 mg) was weighed and sealed in an aluminum pan. The glass transition temperature (T_g) was taken as the midpoint of the heat capacity transition between the upper and lower points of deviation from the extrapolated glass and liquid lines, determined at a scan rate of 20 °C min^{-1} over the temperature range from −50 to −150 °C. A TA Instruments thermogravimetric analyzer, operated at a scan rate of 20 °C over temperatures ranging from 30 to 800 °C under a N_2 purge of 40 mL min^{-1}, was used to record TGA thermograms of samples on a platinum holder. TEM images were recorded using an FEI T12 transmission electron microscope operated with a low-energy electron beam (120 keV). The samples were prepared by placing drops of solutions onto copper grids coated with carbon supporting films and then drying in a vacuum drying machine; staining was performed through exposure to the vapor of 4% aqueous RuO_4 for 30 min. Wide-angle X-ray diffraction (WAXD) measurements were performed using a BL17A1 wiggler beamline at the National Synchrotron Radiation Research Center (NSRRC), Taiwan. For the determination of association constants, NMR spectroscopic titration was employed; a polymeric system and an appropriate deuterated solvent were mixed with various amounts of MD-POSS; NMR spectra were recorded using a Varian Unity Inova 300 FT NMR spectrometer operated at 500 MHz; chemical shifts are reported in ppm. The hydrodynamic diameters of the assemblies were measured by dynamic light scattering (DLS) using a Brookhaven 90 plus instrument (Brookhaven Instruments Corporation, USA) equipped with a He–Ne laser operated at a power of 35 mW at 632.8 nm. All DLS measurements were performed using a wavelength of 632.8 nm at 25 °C and an angle of 90°. Before measurements, the samples were filtered through a Teflon membrane and then the test solution was placed in an appropriate solvent in the DLS cell.

Results and discussion

Synthesis of MD-POSS

We characterized MD-POSS using SEC, ^{1}H and ^{29}Si NMR spectroscopy, MALDI-TOF mass spectrometry, and FTIR spectroscopy. Fig. 1 presents ^{1}H NMR spectra of M(*sec*)A-POSS,

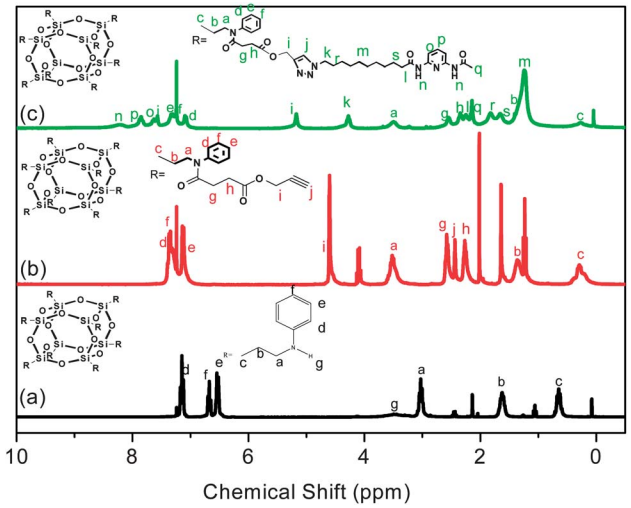

Fig. 1 ^{1}H NMR spectra of (a) M(*sec*A)-POSS, (b) MA-POSS, and (c) MD-POSS in $CDCl_3$.

MA-POSS, and MD-POSS in various deuterated solvents. The broadened peak at 3.48 ppm for the secondary amino proton of M(*sec*)A-POSS [Fig. 1(a)] disappeared and the signal for H_a at 3.04 ppm shifted to 3.52 ppm, with signals appearing at 4.61 and 2.42 ppm for the propargyl group, after the formation of MA-POSS [Fig. 1(b)], consistent with successful amidations. In addition, the signal for MA-POSS near 4.61 ppm was replaced by a signal near 5.16 ppm for MD-POSS [Fig. 1(c)], consistent with successful click reactions.[32] The ratio of the integral values of the proton α to the secondary amino group (H_a, *ca.* 3.51 ppm) and the proton H_i of the ester unit (*ca.* 5.16 ppm) in Fig. 1(c) was approximately 1, consistent with a successful click reaction between each propargyl and azido functional group. In the SEC traces of M(*sec*)A-POSS, MA-POSS, and MD-POSS (Fig. 2), the major signal at an elution time of 16.5 min for M(*sec*)A-POSS shifted to 15.5 min, with no remnant signal, indicating that all of the secondary amino groups of M(*sec*)A-POSS had reacted through amidation to produce MA-POSS. Similarly, the signal that eluted at 15.5 min shifted to 14.5 min, without any remnant peak, suggesting that complete click reactions of MA-POSS had occurred to produce MD-POSS—a compound presenting multiple diaminopyridine functional groups tethered to a POSS cage. We attribute the small shoulders appearing at elution times longer than those of the major peaks in the SEC traces because of the POSS-stationary phase interactions arising from the inter-molecular hydrogen bonding between POSS and DMF solvent. MALDI-TOF mass spectrometry is another general method to characterize the chemical structure of POSS compounds.[33,34] The MALDI-TOF mass spectrum (Fig. S1†) of MD-POSS, recorded using 2,5-dihydroxybenzoic acid as the matrix, featured three distributions of molecular ions for [MD-POSS + Na]$^+$ at 5500, 6876, and 8243 g mol^{-1}, representing a mixture of POSS cages having values of n of 8, 10, and 12, respectively;[35] the signal intensities suggested that most of the POSS cages in the mixture had a value of n of 10 and the minor fraction of oligomers ($n = 8$ and $n = 12$) always exists even *after* attempts to separate them by *chromatographic methods due to strong multiple hydrogen bonding units in this compound.* Fig. S2† presents the ^{29}Si NMR spectrum of the MD-POSS, which shows three resonance bands of the silicon atoms corresponding to the T_8, T_{10} and T_{12} MD-POSS cages at −71.3, −69.1 and −67.3 ppm, respectively. The result is consistent with MALDI-TOF analysis. The FTIR spectra of M(*sec*)A-POSS, MA-POSS, and MD-POSS (Fig. S3†) feature a signal for the Si–O–Si stretching vibration of POSS near 1100 cm^{-1}. The N–H stretching vibration of M(*sec*)A-POSS at 3422 cm^{-1} in Fig. 3(a) disappeared upon forming MA-POSS, with the appearance of alkyne C–H and C≡C, amide, and ester C=O stretching peaks at 3290, 2122, 1741, and 1655 cm^{-1}, respectively. In the spectrum of MD-POSS [Fig. S3(c)†], signals for the free and bound N–H units of the diaminopyridine groups appeared at 3422 and 3290 cm^{-1}, respectively, with no sign of any signal for alkyne C–H groups—confirming the complete reaction of all of the propargyl units. Taken together, the SEC traces and ^{1}H and ^{29}Si NMR, MALDI-TOF, and FTIR spectra all suggested that MD-POSS had been synthesized successfully.

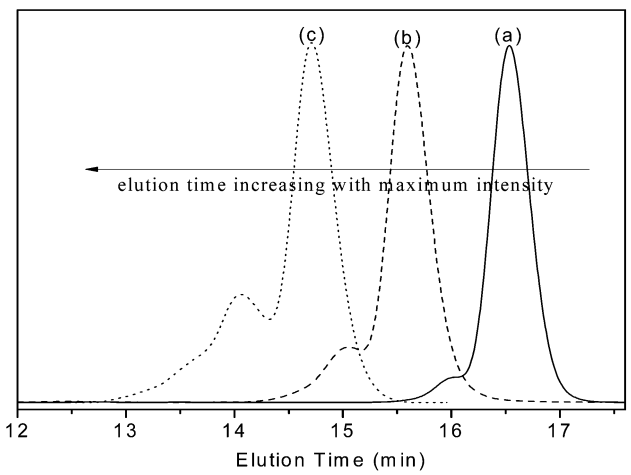

Fig. 2 SEC traces of (a) M(*sec*A)-POSS (solid line), (b) MA-POSS (dashed line), and (c) MD-POSS (dotted line).

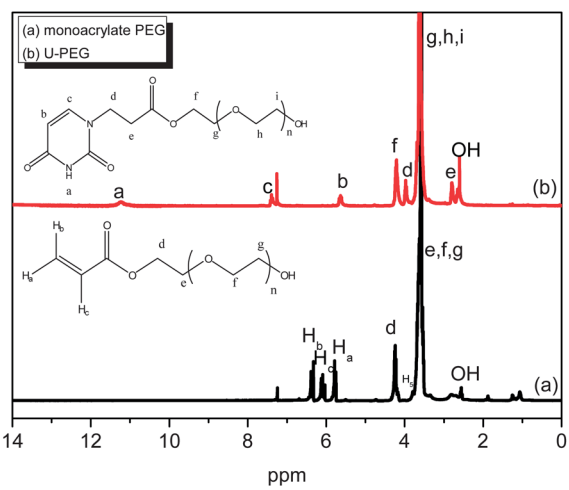

Fig. 3 ^{1}H NMR spectra of (a) acrylate–PEG and (b) U–PEG in $CDCl_3$.

Syntheses of U–PEG and U–PEG–U

Fig. 3 presents ^{1}H NMR spectra of monoacrylate–PEG and U–PEG in $CDCl_3$. Two doublets and a quartet represent the protons of the vinyl group ($1H_b$, $1H_a$, $1H_c$) of monoacrylate–PEG at 6.35, 6.08, and 5.72 ppm, with relative integration of 1 : 1 : 1, corresponding to the iso, trans, and substituted vinyl protons.[36] The signals of the vinylic hydrogen atoms of monoacrylate–PEG are absent in the spectrum of U–PEG, indicating that the starting monomers had been consumed completely; signals at 2.8, 3.95, 5.65, 7.4, and 11.25 ppm, attributable to the protons of the U group, confirmed the successful synthesis of U–PEG. Fig. 4 displays ^{1}H NMR spectra of methacrylate–PEG, methacrylate–PEG–acrylate, and U–PEG–U in $CDCl_3$. The signal for the OH group of methacrylate–PEG at 2.65 ppm in Fig. 4(a) disappeared, with signals appearing at 5.5, 5.75, and 6.0 ppm for the vinyl groups in Fig. 4(b), suggesting the successful synthesis of methacrylate–PEG–acrylate. The ^{1}H NMR spectrum in Fig. 4(c) lacks any of the signals for the methacrylate and acrylate protons of methacrylate–PEG–acrylate in the region from 5.3 to 6.5 ppm; signals appeared, however, for the U rings at 10.3 ppm (amino proton) and at 7.3 and 5.5 ppm, confirming the successful synthesis of U–PEG–U. Fig. S4† presents FTIR spectra of acrylate–PEG, U–PEG, and U–PEG–U in the range from 1500 to 1800 cm^{-1}. The spectrum of acrylate–PEG [Fig. S4(a)†] features a signal at 1640 cm^{-1}, for C=C stretching vibrations, that was absent in the FTIR spectra of U–PEG and U–PEG–U [Fig. S4(b) and (c),† respectively]. GPC and electron impact-mass spectrophotometer (EI-MS) analyses are shown in Fig. S5 and S6,† also indicating that the syntheses of U–PEG and U–PEG–U were successful. Fig. S7† provides DSC thermograms of acrylate–PEG, U–PEG, and U–PEG–U. Acrylate–PEG is a crystalline oligomer having values of T_g, T_c, and T_m of −70, −51, and −5 °C, respectively. Addition of U groups to the PEG caused U–PEG and U–PEG–U to become amorphous, with their values of T_g increasing to −34 and −23 °C, respectively. These data indicate that addition of U—a supramolecular functionalized group that experiences self-complementary interactions—to PEG disrupted the polymer's chain folding and eliminated its crystallinity.

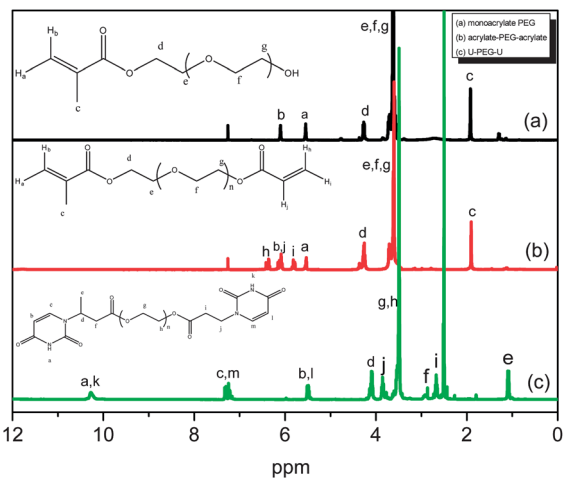

Fig. 4 ^{1}H NMR spectra of (a) acrylate–PEG, (b) acrylate–PEG–acrylate, and (c) U–PEG–U in $CDCl_3$.

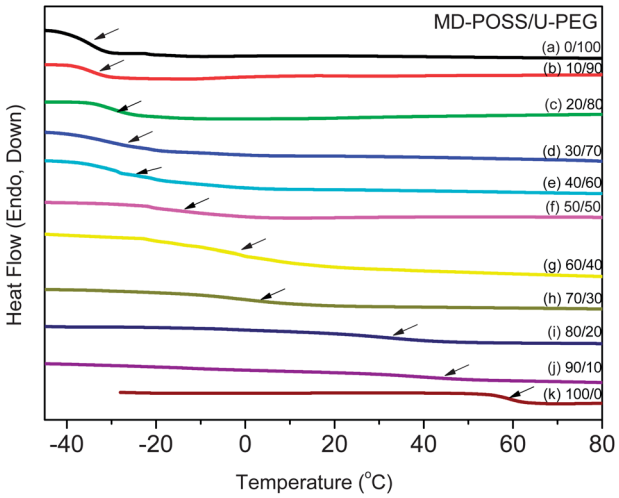

Fig. 5 DSC thermogram of U–PEG/MD-POSS blended systems.

Self-assembly of supramolecular structures from U–PEG and U–PEG–U with MD-POSS

Fig. 5 and 6 present DSC traces of the MD-POSS/U–PEG and MD-POSS/U–PEG–U blends, respectively. When we added MD-POSS to U–PEG and U–PEG–U, the values of T_g of the polymers increased gradually from −34 and −23 °C, respectively, up to approximately 60 °C, depending on the fraction of MD-POSS within the mixture. The increased values of T_g resulted from decreases in the spacing (free volume) between PEG chains, due to the formation of complementary multiple hydrogen bonding interactions between the MD-POSS and U–PEG (U–PEG–U) units. All of the mixtures of MD-POSS/U–PEG and MD-POSS/U–PEG–U exhibited one value of T_g, revealing that the systems were miscible. Fig. S8† summarizes the glass transition

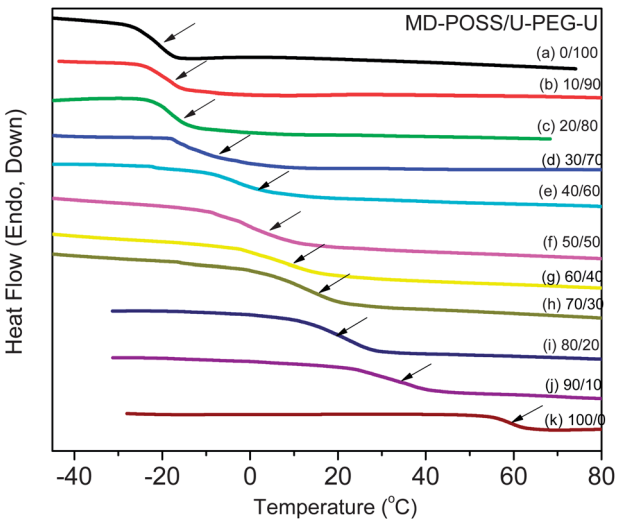

Fig. 6 DSC thermogram of U–PEG–U/MD-POSS blended systems.

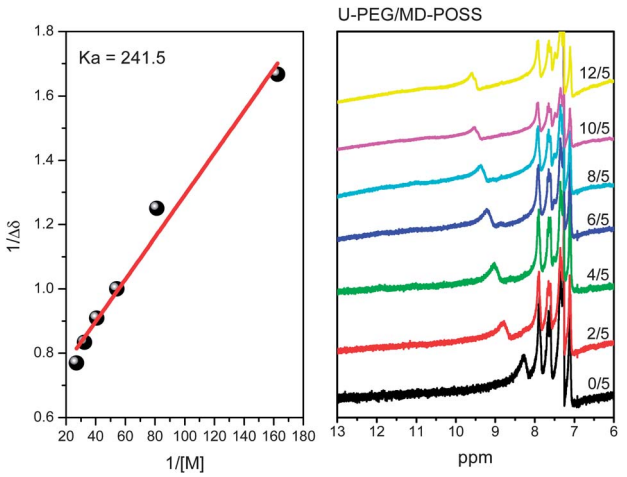

Fig. 7 Association constant data for the U–PEG/MD-POSS blended system.

behaviors of these two supramolecular systems. The value of T_g for MD-POSS/U–PEG–U was greater than that for MD-POSS/U–PEG, implying that complementary multiple hydrogen bonding interactions of the U groups at both chain ends of U–PEG–U were stronger than those at the single chain end of U–PEG.

Fig. 7 and 8 provide plots of NMR titration data and calculations of inter-association equilibrium constants (K_a) for the MD-POSS/U–PEG and MD-POSS/U–PEG supramolecular systems. We used the Benesi–Hildebrand model to calculate the association constants from the NMR spectroscopic titration data. For these calculations, we assumed nonlinear chemical shift data that would be expected for dimeric, hydrogen-bonded associations.[37,38] We used the equation

$$\frac{1}{\Delta\delta} = \frac{1}{(K_a \Delta\delta_{max}[\mathrm{UPEG(UPEGU)} - \mathrm{MDPOSS}])} + \frac{1}{\Delta\delta_{max}}$$

where $\Delta\delta_{max}$ is the maximum change of the chemical shift of the U NH protons corresponding to complete formation of the associated complex. The slope of the double reciprocal plot is $1/K_a\Delta\delta_{max}$ and the intercept is $1/\Delta\delta_{max}$. From the slopes of the plots, we obtained values of K_a of 241.5 M^{-1} for MD-POSS/U–PEG and 1360.8 M^{-1} for MD-POSS/U–PEG–U.[39] These values confirm that strong interactions existed in the MD-POSS/U–PEG and MD-POSS/U–PEG–U systems. The values of K_a for the association events of hydrogen bonded dimers U–U, diamidopyridine–diamidopyridine (DAP–DAP), and uracil–diamidopyridine (U–DAP) are 80, 170, and 800 M^{-1}, respectively.[40] The value of K_a for the MD-POSS/U–PEG–U system was much higher than that for the MD-POSS/U–PEG system because the former features twice the number of U groups as the latter. Because U–PEG possesses only one functional U group per molecule, it can interact with a complementary species from only one side. For U–PEG–U, in contrast, the probability of collisions in the supramolecular interaction mode U–DAP was much higher, resulting in a higher value of K_a.

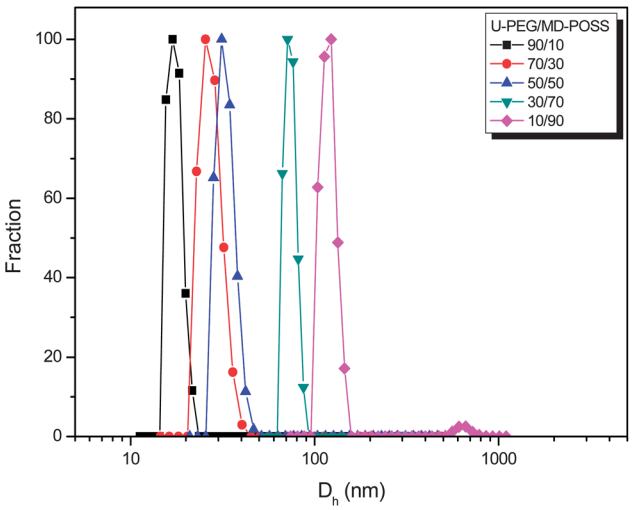

Fig. 9 DLS data for the U–PEG/MD-POSS system.

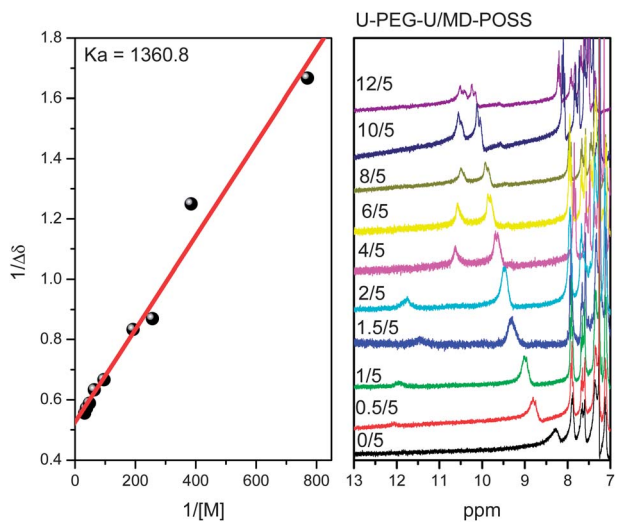

Fig. 8 Association constant data for the U–PEG–U/MD-POSS blended system.

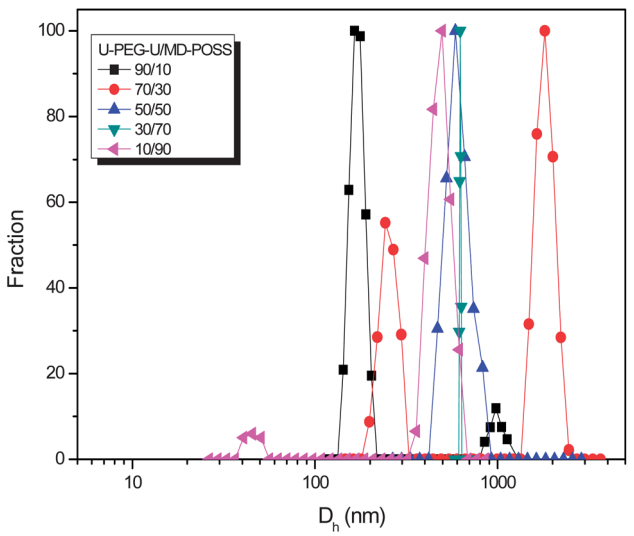

Fig. 10 DLS data for the U–PEG–U/MD-POSS system.

The complementary multiple hydrogen bonding interactions were also evident in FTIR spectra. Fig. S9 and S10† present FTIR spectra (in the 3100–3500 cm^{-1} region) for the supramolecular complexes formed between MD-POSS and U–PEG and U–PEG–U, respectively. We attribute the broad band centered at 3412 cm^{-1} to the free NH units of the DAP moieties of MD-POSS.[40] Its intensity decreased immediately upon increasing the content of U–PEG or U–PEG–U, due to the U groups interacting with the DAP groups. We assign the signals at 3211 and 3273 cm^{-1} to the NH units of the DAP moieties.[41] Moreover, the intensity of the signal in the 3110–3184 cm^{-1} range representing the NH units in U–U dimer interactions decreased upon increasing the amount of MD-POSS; that is, the dimer conformation of the U moieties was disrupted through the insertion of DAP units to form DAP–U interactions. Notably, however, the signal for the NH groups in the U dimers did not disappear completely (at 3184 cm^{-1}), revealing that these U moieties could interact not only with DAP units but also with themselves. The DAP–U interactions were presumably hindered by the huge particle size of MD-POSS.

Fig. S11 and S12† present FTIR spectroscopic data, in the 1600–1800 cm^{-1} range, for mixtures of MD-POSS and U–PEG

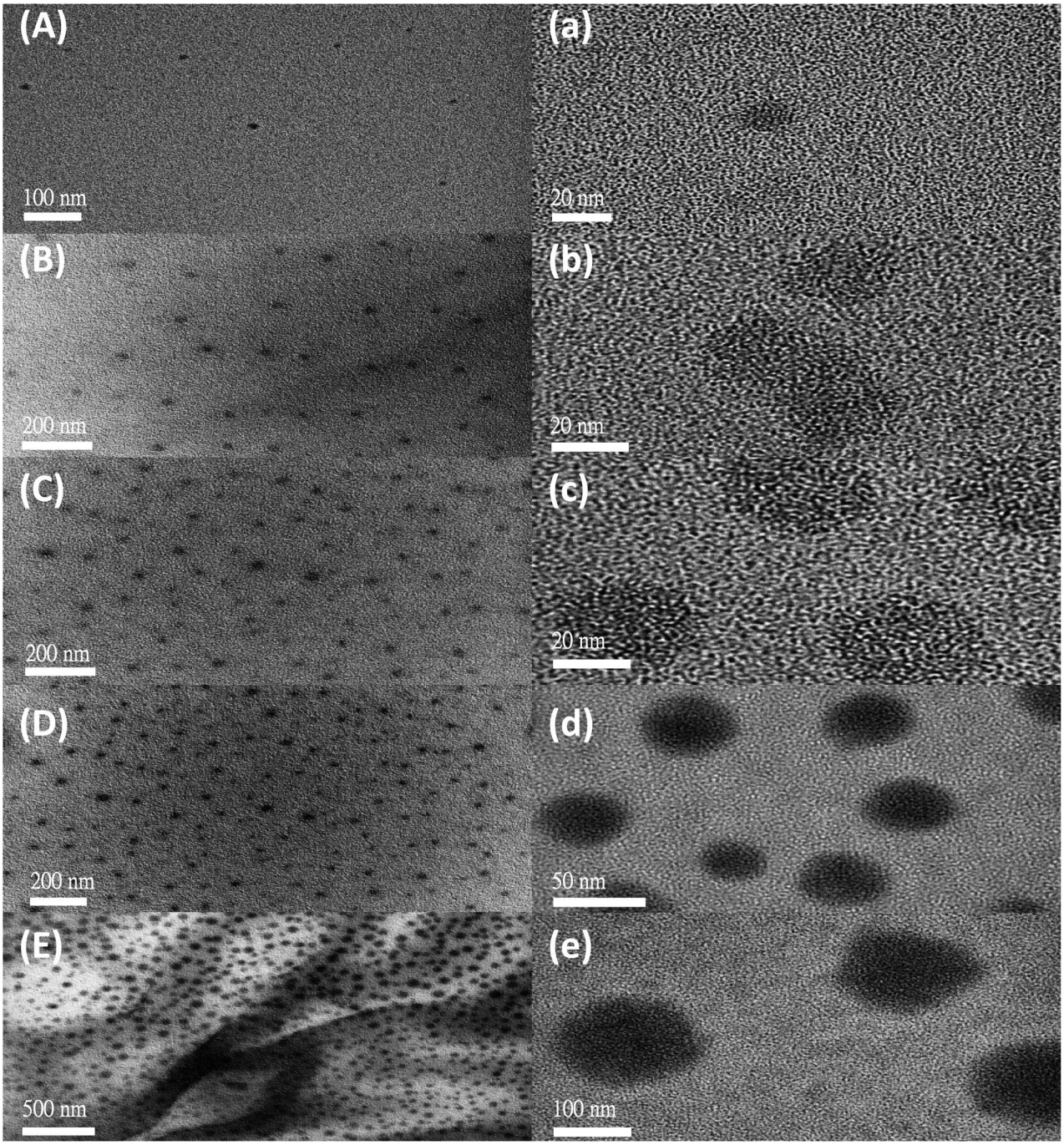

Fig. 11 TEM images for the U–PEG/MD-POSS blend system for (A) 90/10, (B) 70/30, (C) 50/50, (D) 30/70, and (E) 10/90.

and U–PEG–U, respectively. We attribute the signal at 1730 cm^{-1} to the free C═O units in U–PEG, U–PEG–U, and MD-POSS; its unchanging position suggests that the C═O groups near the ethylene oxide units in U–PEG and U–PEG–U and between the secondary amine and triazole-aromatic rings in MD-POSS did not interact through hydrogen bonding with either the U or DAP moieties. The intensity of the signal at 1710 cm^{-1}, which we attribute to the free C═O groups of the U moieties in each system, decreased upon increasing the content of MD-POSS, suggesting that the U moieties interacted with other groups. The intensity of the signal at 1670 cm^{-1}, representing the bound C═O groups in the U dimer, decreased upon adding MD-POSS to U–PEG or U–PEG–U, confirming that the U dimer was disrupted in the presence of MD-POSS, consistent with Fig. S8 and S9.†

Fig. S13 and S14† present WAXD patterns of U–PEG, U–PEG–U, and their blends with MD-POSS. The patterns for both U–PEG and U–PEG–U feature an amorphous halo at a value of 2θ of 13.3°, consistent with the observation of amorphous structures in their DSC analyses. When we incorporated MD-POSS into U–PEG and U–PEG–U, the bands of their amorphous halos shifted slightly to higher angles, corresponding to slight increases in the intermolecular spacing upon successful insertion of MD-POSS. Although the intermolecular spacing increased, the supramolecular interactions decreased the chain mobility and increased the value of T_g. In addition, the broad band appeared (Fig. S13†) in the pattern for U–PEG, centered at a value of 2θ of 4.2°, caused by the self-complementary U–U interactions; this signal became smaller and broader upon the formation of supramolecular interactions with MD-POSS, again confirming its successful incorporation. Notably, the signals of the amorphous halo for the MD-POSS/U–PEG = 50/50 system were relatively sharp, indicating the existence of a relatively ordered structure.

Fig. 9–12 display DLS data and TEM images of MD-POSS/U–PEG and MD-POSS/U–PEG–U blends. Pointed arrayed structures of aggregated pure MD-POSS, with an average center-to-center distance of 2 μm, are usually formed through dewetting processes during solvent evaporation.[42] Micrometer-sized structures can arise as a result of evaporation-driven instability of hole nucleation.[43,44] For our MD-POSS/U–PEG supramolecular mixtures (Fig. 11), we observe some large and small agglomerations—but all of them are homogeneous. As mentioned above, the presence of a single functional U group in U–PEG results in the U moieties interacting with one another, but the number of interaction sites is too low to ensure formation of the network constructed in the MD-POSS/U–PEG–U system. In the images of the big and small clusters, the high contrast regions, resulting from RuO_4 staining of the aromatic functional groups of the MD-POSS moieties, revealed a new balance between U–U, U–DAP, and DAP–DAP interactions. From the values of K_a (241.5 M^{-1} for the MD-POSS/U–PEG system; 1360.8 M^{-1} for the MD-POSS/U–PEG–U system), we suspect that the rate of formation of the U–DAP interaction was much slower than that of U–U and DAP–DAP modes, due to the smaller content of U groups on each PEG main chain per mole of U–PEG, resulting in the larger probability of DAP–DAP

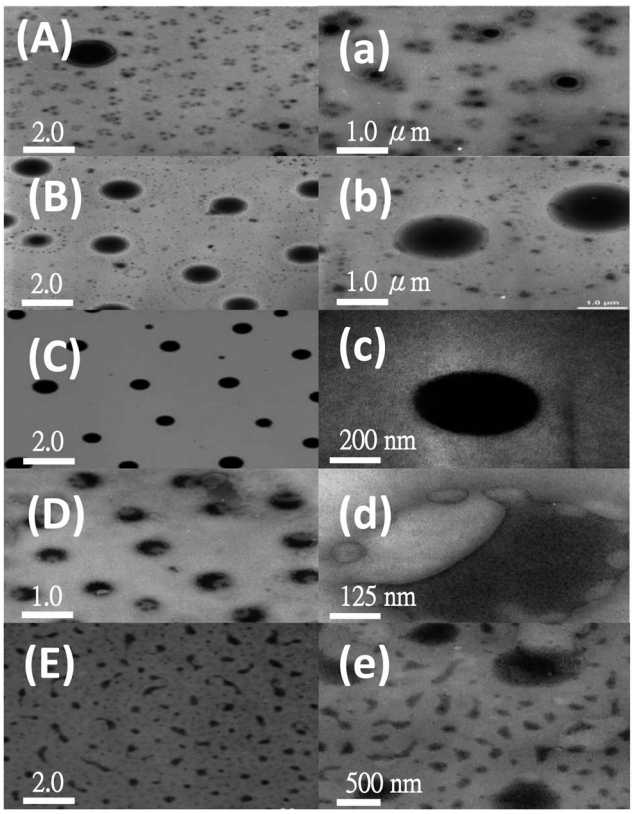

Fig. 12 TEM images for the U–PEG–U/MD-POSS system for (A) 90/10, (B) 70/30, (C) 50/50, (D) 30/70, and (E) 10/90.

interactions, even though the U–DAP mode is theoretically much stronger than either the U–U or U–DAP mode. In Fig. 11, the larger clusters were aggregates of MD-POSS units formed mostly through DAP–DAP hydrogen bonding interactions; the smaller clusters also featured DAP–DAP interactions of MD-POSS units, but the effects were much weaker, meaning that the U–U and U–DAP modes of interaction were relatively stronger than in the larger clusters, as indicated in Scheme 3. Different ratios of MD-POSS did not appear to affect the cluster size; DLS data suggested that all of the clusters had sizes of several hundred nanometers (Fig. 9).

The situation for the MD-POSS/U–PEG–U blends (Fig. 12) differed from that in Fig. 11. Again, many large high-contrast clusters were formed by the MD-POSS units, even though the value of K_a for the U–PEG–U/MD-POSS blend system was much higher than that (1360.8 M^{-1}) for the MD-POSS/U–PEG system. The double number of U groups on each PEG chain per mole of U–PEG–U resulted in greater probabilities for U–DAP interactions among the three kinds of hydrogen bonding modes displayed in Scheme 3. Accordingly, a smaller total cluster size of the U–PEG/MD-POSS system, compared with the MD-POSS/U–PEG–U system, is obvious. Because of the three kinds of hydrogen bonding modes, the MD-POSS/U–PEG–U blend system was more balanced than the MD-POSS/U–PEG system, resulting in a lower probability of MD-POSS aggregation. The cluster size increased upon increasing the content of MD-POSS in the blend system because of the higher probability of

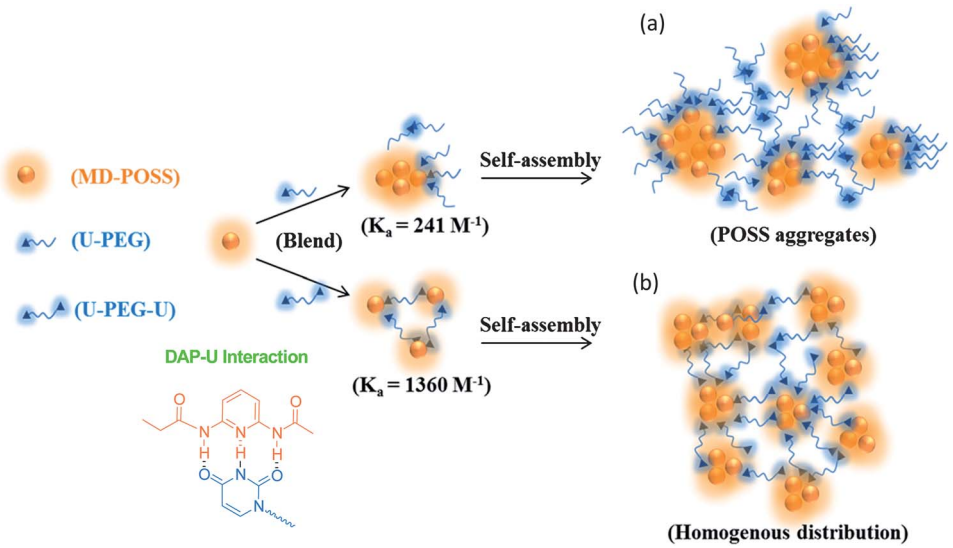

Scheme 3 Multiple hydrogen bonding interactions and possible morphologies of (a) MD-POSSS/U–PEG and (b) MD-POSS/U–PEG–U supramolecular structures.

DAP–DAP interactions. In general, the MD-POSS/U–PEG–U blend systems featured network-like morphologies with more-homogeneous clusters, ranging in size from 15 to 100 nm, relative to those of the MD-POSS/U–PEG systems. The DLS data (Fig. 10) suggested that the cluster size for each ratio of the blend system was slightly larger than that in the TEM image, due to the shrinking that occurred upon evaporating the solvent (THF). Scheme 3 presents the multiple hydrogen bonding interactions and possible morphologies of the systems formed from blends of MD-POSS with U–PEG and U–PEG–U. For the U–PEG system, the association constant is large, resulting in strong interactions between the U and DAP units, in addition to small amounts of U–U interactions between pairs of U–PEG molecules. The association constant for the U–PEG–U system was much greater than that of the U–PEG system, resulting in mostly one type of interaction: U–DAP. Therefore, the MD-POSS/U–PEG–U system formed a strong net-like cluster morphology (confirmed through TEM imaging) because of the much higher probability of U–DAP interactions with two functional U groups present per U–PEG–U molecule; the morphology was also strongly dependent on the mode of hydrogen bonding.

Conclusions

In this study, we synthesized MD-POSS through click chemistry and U-functionalized PEG derivatives through Michael additions. TGA and DSC data revealed that the MD-POSS/U–PEG and MD-POSS/U–PEG–U systems exhibited significantly improved thermal properties as a result of strong complementary multiple hydrogen bonding interactions between the U and DAP moieties. TEM imaging indicated that the interactions in the U–PEG–U systems were relatively stronger and that their structures were relatively more ordered. In addition, the presence of U functional groups and their interactions with MD-POSS transformed the crystalline PEG into completely amorphous complexes. As a possible mechanism for the self-assembly processes occurring in this study, we propose that the U–PEG/MD-POSS systems featured strong interactions between their U and DAP moieties, with relatively lower amounts of U–U dimers; in contrast, the U–PEG–U/MD-POSS systems featured mostly a single type of interaction: U–DAP hydrogen bonding.

Acknowledgements

This study was supported financially by the National Science Council, Taiwan, Republic of China, under contracts NSC 100-2221-E-110-029-MY3 and NSC 101-2628-E-110-003.

References

1 J. M. Plooino and M. Weck, *Chem. Soc. Rev.*, 2005, **34**, 193–207.
2 C. Wang, S. Yang, X. Yu, J. X. Zheng, J. Ma, J. Xu and M. Zhu, *Soft Matter*, 2012, **8**, 10307–10313.
3 M. C. Stuparu, A. Khan and C. J. Hawker, *Polym. Chem.*, 2012, **3**, 3033–3044.
4 Y. C. Wu and S. W. Kuo, *J. Mater. Chem.*, 2012, **22**, 2982–2991.
5 W. H. Binder and R. Zirbs, *Adv. Polym. Sci.*, 2007, **201**, 1–78.
6 A. Muller, F. Talbot and S. Leutwyler, *J. Am. Chem. Soc.*, 2002, **124**, 14486–14494.
7 S. W. Kuo and S. T. Tsai, *Macromolecules*, 2009, **42**, 4701–4711.
8 C. A. Mirkin, R. L. Letsinger, R. C. Mucic and J. J. Storhoff, *Nature*, 1996, **382**, 607–609.
9 K. K. Jain, *Science*, 2001, **294**, 621–623.
10 S. W. Kuo, *Polym. Int.*, 2009, **58**, 455–464.
11 Y. Inaki, *Prog. Polym. Sci.*, 1992, **17**, 515–570.
12 W. T. Smith, *Prog. Polym. Sci.*, 1996, **21**, 209–253.
13 P. Bauerle and A. Emge, *Adv. Mater.*, 1998, **10**, 324–330.
14 A. Khan, D. M. Haddleton, M. J. Hannon, D. Kukulj and A. Marsh, *Macromolecules*, 1999, **32**, 6560–6564.

15 Y. C. Wu, Y. S. Wu and S. W. Kuo, *Macromol. Chem. Phys.*, 2013, **214**, 563–571.
16 A. Bertrand, F. Lortie and J. Bernard, *Macromol. Rapid Commun.*, 2012, **33**, 2062–2091.
17 Y. C. Wu and S. W. Kuo, *Polym. Chem.*, 2012, **3**, 3100–3111.
18 I. H. Lin, C. C. Cheng, Y. C. Yen and F. C. Chang, *Macromolecules*, 2010, **43**, 1245–1252.
19 S. Trakhtenberg, J. C. Warner, R. Nagarajian, F. F. Bruno and L. A. J. Samuelson, *Chem. Mater.*, 2006, **18**, 2873–2878.
20 K. Saito, L. R. Ingalls, J. Lee and J. C. Warner, *Chem. Commun.*, 2007, **24**, 2503–2505.
21 S. W. Kuo and F. C. Chang, *Prog. Polym. Sci.*, 2011, **36**, 1649–1696.
22 Y. Li, X. H. Dong, K. Guo, Z. Wang, Z. C. Wesdemiotis, R. P. Quirk, W. Zhang and S. Z. D. Cheng, *ACS Macro Lett*, 2012, **1**, 834–839.
23 W. Zhang and A. H. E. Muller, *Macromolecules*, 2010, **43**, 3148–3152.
24 J. L. He, K. Yue, Y. Q. Liu, X. F. Yu, P. H. Ni, K. A. Cavicchi, R. P. Quirk, E. Q. Chen, S. Z. D. Cheng and W. B. Zhang, *Polym. Chem.*, 2012, **3**, 2112–2120.
25 E. Gungor, C. Bilir, H. Durmaz, G. Hizal and U. Tunca, *J. Polym. Sci., Part A: Polym. Chem.*, 2009, **47**, 5947–5953.
26 K. Pielichowaski, J. Niuguna, B. Janowski and J. Pielichowski, *Adv.Polym. Sci.*, 2006, **201**, 225–296.
27 S. W. Kuo, H. F. Lee, W. J. Huang, K. U. Jeong and F. C. Chang, *Macromolecules*, 2009, **42**, 1619–1626.
28 Y. C. Lin and S. W. Kuo, *Polym. Chem.*, 2012, **3**, 162–171.
29 E. Jeoung, J. B. Carroll and V. M. Rotello, *Chem. Commun.*, 2002, 1510–1511.
30 J. B. Carroll, A. J. Waddon, H. Nakade and V. M. Rotello, *Macromolecules*, 2003, **36**, 6289–6291.
31 C. C. Cheng, Y. C. Yen and F. C. Chang, *Macromol. Rapid Commun.*, 2011, **32**, 927–932.
32 Y. C. Lin and S. W. Kuo, *Polym. Chem.*, 2012, **3**, 882–891.
33 Y. Li, W. B. Zhang, I. F. Hsieh, G. Zhang, Y. Cao, X. Li, C. Wesdemiotis, B. Lotz, H. Xiong and S. Z. D. Cheng, *J. Am. Chem. Soc.*, 2011, **133**, 10712–10715.
34 J. Xu, X. Li, C. M. Cho, C. L. Toh, L. Shen, K. Y. Mya, X. Lu and C. He, *J. Mater. Chem.*, 2009, **19**, 4740–4745.
35 Y. C. Sheen, C. H. Lu, C. F. Huang, S. W. Kuo and F. C. Chang, *Polymer*, 2008, **49**, 4017–4024.
36 W. H. Hu, K. W. Huang and S. W. Kuo, *Polym. Chem.*, 2012, **3**, 1546–1554.
37 L. Fielding, *Tetrahedron*, 2000, **56**, 6151–6170.
38 N. Mesplet, P. Morin and J. P. Ribet, *Eur. J. Pharm. Biopharm.*, 2005, **59**, 523–526.
39 A. S. Karikari, B. D. Mather and T. E. Long, *Biomacromolecules*, 2007, **8**, 302–308.
40 A. J. Wilson, *Soft Matter*, 2007, **8**, 409–425.
41 Z. Sideratou, D. Tsiourvas, C. M. Paleos, E. Peppas, J. Anastassopoulou and T. Theophanides, *J. Mol. Struct.*, 1999, **484**, 91–101.
42 R. S. Shih, C. H. Lu, S. W. Kuo and F. C. Chang, *J. Phys. Chem. C*, 2010, **114**, 12855–12862.
43 S. L. Tripp, S. V. Pusztay, A. E. Ribbe and A. Wei, *J. Am. Chem. Soc.*, 2002, **124**, 7914–7915.
44 P. C. Ohara and W. M. Gelbart, *Langmuir*, 1998, **14**, 3418–3424.

